Large Transverse Piezoelectricity in Highly (001)-Oriented PZT Thick Films on Titanium Substrates

Zefeng Guo , Jun Ouyang * , Shijing Chen , Zhenyan Liang , Hongbo Cheng *

Posted Date: 21 April 2026

doi: 10.20944/preprints202604.1515.v1

Keywords: PZT film; titanium; (001) orientation; transverse piezoelectric coefficient/$e_{31,f}$; RF magnetron sputtering; rapid thermal processing (RTP); piezo-MEMS

 doi:10.20944/preprints202604.1515.v1

Article

Large Transverse Piezoelectricity in Highly (001)-Oriented PZT Thick Films on Titanium Substrates

Zefeng Guo [1], Jun Ouyang [2,*], Shijing Chen [3], Zhenyan Liang [1] and Hongbo Cheng [1,*]

[1] School of Chemistry and Chemical Engineering, Qilu University of Technology, Jinan 250353, China
[2] Department of Physics, Seton Hall University, South Orange, NJ, 07079, USA
[3] Hunan Provincial Key Laboratory of Thin Film Materials and Devices, School of Materials Science and Engineering, Xiangtan University, Xiangtan 411105, China
* Correspondence: jun.ouyang@shu.edu (J.O.); hbc@qlu.edu.cn (H.C.)

Abstract

Integration of lead zirconate titanate (PZT) films on metallic substrates is important for flexible piezoelectric devices, but achieving highly textured crystallinity without detrimental interfacial diffusion or oxidation remains challenging. In this work, PZT thick films (~1.3 μm) were deposited on titanium substrates using radio-frequency magnetron sputtering at 400 °C followed by rapid thermal processing at 640 °C for 2.5 min. A conductive $LaNiO_3$ buffer layer was introduced to promote nucleation of the perovskite phase and suppress interfacial degradation. The resulting PZT films on LNO/Pt/Ti substrates exhibit a strong (001) preferred orientation and dense microstructure. The films show a large remnant polarization Pr of ~61 μC cm^{-2} and a low coercive field E_c of ~56 kV cm^{-1} at 60 V, together with dielectric constants ε_r of ~1350–1612 and dielectric loss tanδ ≤ 0.06 in the frequency range of 1 kHz–1 MHz. Patterned Pt/PZT/LNO/Pt/Ti cantilevers yield a transverse piezoelectric coefficient $e_{31,f}$ of ~ –6.7 C m^{-2}, significantly outperforming reported piezoelectric films deposited on Ti. These results demonstrate that controlled nucleation and rapid thermal crystallization enable highly textured PZT films on reactive metallic substrates, providing a viable route for flexible piezoelectric MEMS devices.

Keywords: PZT film; titanium; (001) orientation; transverse piezoelectric coefficient/$e_{31,f}$; RF magnetron sputtering; rapid thermal processing (RTP); piezo-MEMS

1. Introduction

Lead zirconate titanate (PZT) films, particularly those with morphotropic phase boundary (MPB) compositions [1], have established themselves as the cornerstone of piezoelectric micro-electro-mechanical-systems (Piezo-MEMS) due to their exceptional electromechanical properties. While silicon-based PZT film devices have been extensively investigated [2–5], the intrinsic brittleness of silicon limits their use in emerging flexible electronic systems such as wearable sensors, flexible actuators and vibrational energy harvesters. In contrast, metallic foils have recently attracted increasing attention as substrates for flexible electronics because of their mechanical ductility, durability, and relatively low cost. Among various metallic substrates, titanium (Ti) is particularly attractive for the integration of PZT films. One important advantage is the close match between the coefficient of thermal expansion (CTE) of Ti (~8.6×10^{-6} $°C^{-1}$) and that of PZT (~8.0×10^{-6} $°C^{-1}$) [6], which helps reduce thermally induced stresses that may otherwise degrade film integrity or cause delamination during processing. In addition, titanium exhibits excellent corrosion resistance, high toughness, and good manufacturability, making it a promising platform for flexible functional thin-film devices.

 doi:10.20944/preprints202604.1515.v1

Despite these advantages, the integration of high-quality PZT films on Ti substrates remains challenging. Previous investigations via common deposition methods, like sputtering or sol-gel [7–9], have consistently shown that, achieving a pure perovskite phase with an epitaxial quality or a high texture in a PZT film, requires a prolonged exposure to a high processing temperature (typically exceeding 500 °C) in an O_2-rich atmosphere (for suppressing the formation of oxygen vacancies). In such a chemical environment, the highly reactive Ti substrate readily undergoes an interfacial diffusion and a severe oxidation, resulting in the formation of a low-permittivity interfacial oxide layer [10–12], or the decomposition of PZT into a non-ferroelectric pyrochlore phase [10]. Both effects significantly degrade the electrical performance of the PZT film [10,11]. Consequently, reducing the thermal budget during film processing is essential for preserving interfacial stability while enabling high-quality PZT growth on Ti substrates.

A two-step processing strategy combining low-temperature deposition with rapid thermal processing (RTP) has been proposed to address this challenge. In this approach, PZT is first deposited at a relatively low temperature and subsequently crystallized through a rapid high-temperature annealing step, thereby minimizing the thermal exposure of the Ti substrate. However, an additional challenge arises in achieving the highly desirable (001) crystallographic texture in PZT films deposited on metallic substrates. The large lattice mismatch between (001)-oriented PZT and conventional metallic electrodes such as Pt or Ti typically results in randomly oriented polycrystalline films [6,10], which exhibit reduced piezoelectric performance. Introducing a suitable buffer layer that provides a crystallographic template for the nucleation and growth of (001)-oriented PZT is therefore critical.

In this work, we demonstrate an optimized two-step fabrication route for producing highly (001)-textured PZT thick films on titanium substrates. The process combines RF magnetron sputtering at 400 °C with rapid thermal processing, together with the introduction of a conductive $LaNiO_3$ (LNO) buffer layer. The LNO layer serves as a structural template that promotes the nucleation and growth of perovskite PZT while mitigating lattice mismatch with the underlying substrate [13–15]. In addition, it acts synergistically with the RTP process to suppress interfacial diffusion. As a result, the PZT films grown on LNO/Pt/Ti substrates exhibit a strong (001) preferred orientation and dense microstructure, yielding a high remanent polarization P_r of ~61 μC cm^{-2} and a large transverse piezoelectric coefficient $e_{31,f}$ of –6.7 C m^{-2}. These results demonstrate that controlled interfacial nucleation combined with rapid thermal crystallization enables the formation of highly textured PZT films on reactive metallic substrates.

2. Materials and Methods

2.1. Film Fabrication

In this study, PZT films with a Zr/Ti atomic ratio of 52/48 were fabricated on $LaNiO_3$ (LNO) buffered Pt/Ti substrates. Titanium substrates (TA1 grade, >99.5% purity, wool wheel polished, 20*10*0.5 mm) with a Young's modulus of 104 GPa [16] were used. The PZT/LNO/Pt/Ti thin film hetero-structures were prepared in a multi-target magnetron sputtering system equipped with 3-inch sputtering guns, and a base pressure of 2.0×10^{-4} Pa was achieved prior to film deposition. The ceramic PZT target (99.9% purity) was purchased from Hefei Kejing Materials Technology Co., Ltd. (Hefei, China), with a 20 mol% excessive PbO to compensate for the volatilization loss of lead during target sintering and film processing. A chemically stoichiometric LNO ceramic target (99.9% purity) was supplied by Hefei Anjing Crystal Material Co., Ltd. (Hefei, China), while the Pt and Ti metallic targets (99.99% purity) were purchased from ZhongNuo Advanced Material Technology Co., Ltd., (Beijing, China). A Pt bottom electrode (~300 nm), with a Ti adhesion layer (~ 10 nm), was firstly sputtered onto the Ti substrate at 300 °C in pure Ar at a pressure of 0.3 Pa. The sputtering power for both Pt and Ti was 55 W. Secondly, a LNO buffer layer (~120 nm thick) was deposited at 400 °C with a RF power of 100 W from its ceramic target, in an Ar/O_2 mixed atmosphere (4:1 flow ratio) at a pressure of 0.3 Pa. Lastly, a PZT thick film (~ 1.3 μm) was deposited onto the LNO layer from its ceramic target,

 doi:10.20944/preprints202604.1515.v1

at the same temperature of 400 °C and in the same Ar/O2 atmosphere, but at a higher sputtering pressure of 1.2 Pa. The detailed deposition parameters are summarized in Table 1. The as-deposited films were annealed via rapid thermal processing (RTP) in an oxygen atmosphere (1.2 L/min fixed flow rate), using a RTP-300 furnace purchased from Beijing East-Star Applied Physics Research Institute (Beijing, China). The RTP process involved ramping from room temperature to 640 °C at a rate of 2.5 °C/s, followed by a holding time of 2.5 min. The annealed films were then cooled down to room temperature by switching off the RTP furnace.

Table 1. Process parameters for the sputter-deposition of PZT/LNO/Pt/Ti heterostructures.

Layers	Ti (adhesion)	Pt	$LaNiO_3$	$Pb(Zr,Ti)O_3$
Base pressure (Pa)		2.0×10^{-4}		
Target-substrate distance (mm)		50		
Target diameter (inches)		3		
Substrate temperature (◦C)	300		400	
Sputtering pressure (Pa)	0.3		0.3	1.2
Sputtering power (W)	55		100	130
Sputtering atmosphere	Ar		Ar/O_2~4:1	
Targeted thickness (nm)	10	300	120	1300

2.2. Characterization

The crystallographic characteristics, including phase structure, crystalline orientation and quality of the PZT films, were investigated using X-ray diffraction (XRD) in a SmartLab 9kW diffractometer (Rigaku, Japan). For surface morphology analysis, atomic force microscopy (AFM) was carried out using an AFM 100Plus microscope (Hitachi. Japan). Cross-sectional nanoscale structural and chemical composition analyses were performed via transmission electron microscopy (TEM) in a Talos F200X electron microscope (Thermo Fisher Scientific, USA) equipped with an Energy Dispersive Spectrometer (EDS). For electrical measurements, Au top electrodes (200 μm in diameter) were deposited on the PZT film surface via DC sputtering through a shadow mask in a SBC-12 vacuum sputter (KYKY, China). The dielectric properties were assessed using a TH2838H precision LCR meter (Tonghui, China). Leakage current density, polarization-electric field (*P-E*) hysteresis loops, and the corresponding switching currents were measured using a MultiferroicTM ferroelectric tester (Radiant Technology, USA).

The transverse piezoelectric coefficients ($e_{31,f}$) were determined by measuring the tip displacements of a PZT film cantilever. A Pt/PZT/LNO/Pt/Ti heterostructure, with the Pt top electrode being deposited via RF magnetron sputtering at room temperature, was diced into cantilever beams with dimensions of 20 mm (length) × 3 mm (width) × 0.5 mm (thickness). The Pt top electrode was connected to a function generator via a fine gold wire, through which a sinusoidal ac voltage was applied to actuate the cantilever. The resulting tip displacements (δ) of the PZT film cantilever were measured using a Laser Doppler Vibrometer (LDV) comprising an OFV-505 sensor head and an OFV-5000 controller (Polytec Inc., USA). Detailed information regarding the fabrication and testing procedures of the piezoelectric film cantilevers can be found in a previous report [14].

3. Results

The bedrock of our strategy is to decouple the crystallization step, which can be rapidly achieved at a high temperature with a LNO template, from the PZT film deposition, which demands a long time period and should be carried out at a low temperature. Such a strategy has successfully passivated the Ti and O diffusions, i.e., preventing Ti from penetrating into the PZT layer and

 doi:10.20944/preprints202604.1515.v1

minimizing oxidation of the Ti substrate. Figure 1a presents the XRD 2-scan patterns of the PZT film before and after RTP, which unequivocally demonstrate the effectiveness of this two-step approach. The as-deposited film, grown at a low temperature of 400 °C, exhibits some residue PbO crystallites due to a suppressed lead volatilization, as well as a poorly crystallized perovskite structure with a (101) preferred orientation. The latter can be attributed to a surface energy-dictated nucleation & growth process at low-temperature, with the (101) plane having a minimal surface energy in perovskite oxides. These observations are consistent with our previous results [17]. In contrast, a dramatic microstructure change occurred after the RTP treatment (@640 °C for just 2.5 minutes). The film evolved into a pure perovskite phase, evidenced by the disappearance of the PbO peak. More importantly, it displayed a highly crystalline (001)-texture. This crystalline reorientation is a direct consequence of hetero-structure engineering. Firstly, a (100)-oriented nucleation and growth was promoted in the as-grown and RTP-annealed LNO film [18,19]. Secondly, with a pseudo-cubic perovskite structure and a close lattice match to (001) PZT, the (100)-oriented LNO film acted as a crystallographic template [14,19], providing a thermodynamically favorable pathway for (001)-oriented growth of the PZT film, especially during the high-temperature recrystallization process driven by RTP. The formation of this (001) texture is essential, as this crystallographic orientation aligns with the spontaneous polarization axis in tetragonal PZT, thereby demonstrating superior ferroelectric and piezoelectric performances [20,21].

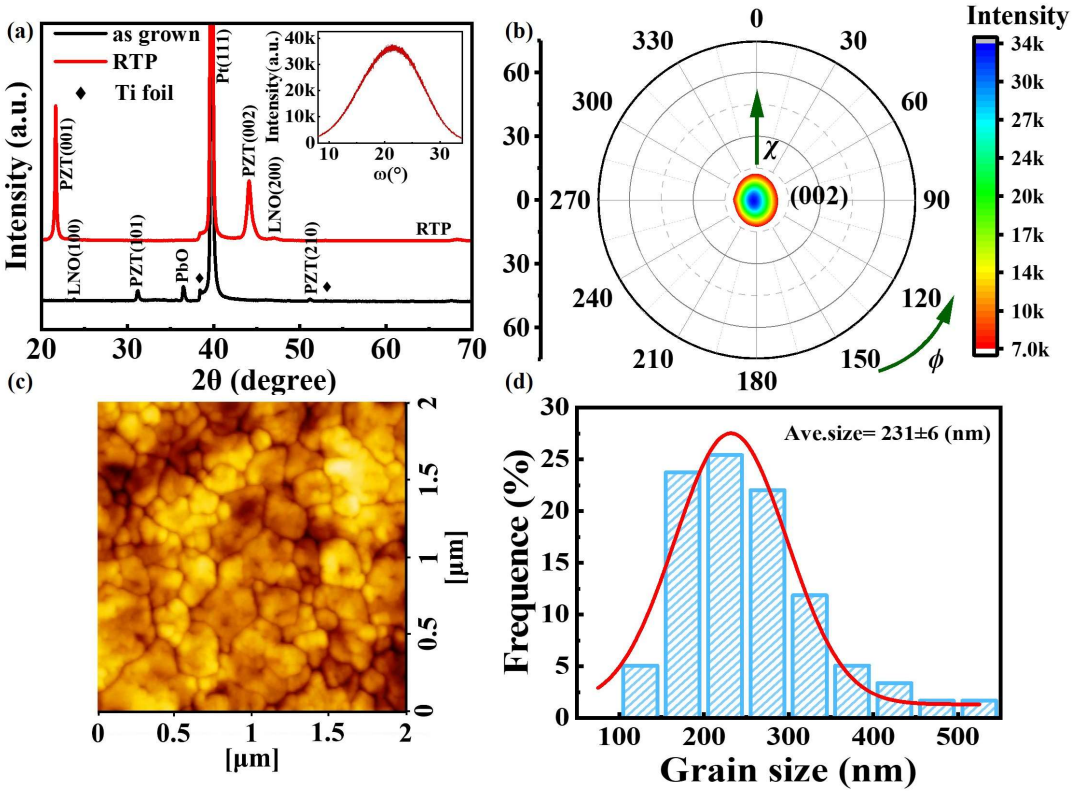

Figure 1. Crystalline phase structure and surface analyses of $Pb(Zr_{0.52}Ti_{0.48})O_3$ (PZT) films grown on $LaNiO_3$ (LNO)-buffered Pt/Ti substrates: (a) XRD 2θ-scan patterns of the PZT film before and after RTP, with the inset showing the rocking curve of the RTP-treated film in the (002) plane; (b) XRD pole figure of the (002) PZT peak, (c) AFM surface scan image and (d) histogram of the in-plane grain diameter for the RTP-treated PZT film.

To evaluate the crystalline quality of the resulted PZT film, an XRD rocking curve was acquired for the (002) PZT peak (inset of Figure 1a). The symmetric peak with a maximum count exceeding 30k and a full-width at half-maximum (FWHM) of approximately 6°, confirms a good (001)-textured crystallinity. Furthermore, an XRD pole figure for the (002) PZT peak, shown in Figure 1b, provides

 doi:10.20944/preprints202604.1515.v1

a 3D rendering of the (00l) texture. The diffraction intensity is highly concentrated near the center of the pole figure (χ ranges from 0° to ~ 12°) with no other detectable peaks, indicating that the c-axes of the PZT grains in the film are either aligned with or within a small angle to the film normal. An AFM image showing the film's surface morphology was given in Figure 1c, which reveals a dense film surface with in-plane equiaxial grains. A low root-mean-square (RMS) roughness of ~7.7 nm and an average in-plane grain diameter of ~231 ± 6 nm (Figure 1d) over a 5×5 μm^2 scanning area further attest to the smoothness and high crystalline quality of the film. These features are essential for a reliable electrical performance.

TEM analyses were performed to investigate the nanoscale structural and chemical composition characteristics. Figure. 2a is a low-magnification cross-sectional bright field TEM image of the PZT/LNO/Pt/Ti heterostructure. No delamination is observed across the interfaces, suggesting a good adhesion throughout the multilayer stack. The PZT film (~1.27 μm) exhibits a dense columnar microstructure free of macroscopic defects such as large pores or cracks. It does show a small amount of nanopores (white dots in the image) due to the RTP process [22]. However, these pores are mostly isolated due to the short period of high temperature exposure, therefore they are not expected to deteriorate the electrical performance of the PZT film [22]. The PZT/LNO/Pt/Ti heterostructure shows clear variations in the microstructures of the consisting layers and interfaces. The Ti/Pt interface is rough and mechanically interlocked by a transition layer (the dark gray layer sandwiched between the Pt bottom electrode and the Ti substrate), which is ~ 100 nm thick and can be attributed to a thermal interdiffusion of the two metallic layers. Moreover, near the center of the Pt layer, which shows a deep dark gray contrast with a textured columnar grain morphology, there are embedded, semi-continuous light gray regions. These regions demonstrate the same contrast as that of the Ti substrate, indicating that they might be rich in thermally diffused Ti. The latter has been reported to occur at an elevated temperature through the grain boundaries of a Pt layer and get oxidized inside it [12].

To further investigate the PZT/LNO interface at the nanoscale, high-resolution TEM (HRTEM) imaging was performed and the result is shown in Figure 2b. An atomically sharp boundary is observed between the two highly crystalline layers with no detectable secondary phases or amorphous "dead zone", which are usually caused by interdiffusion. This confirms that the LNO layer acts not only as a crystallographic template, but also as a robust diffusion barrier, preventing the downward diffusion of Pb, Zr or Ti from the PZT film. Furthermore, to estimate the lattice distortion of the PZT film, high-magnification lattice imaging was performed on selected regions of Figure 2a, revealing a highly ordered atomic arrangement, as shown in Figures 2c and 2d. Fast Fourier Transform (FFT) analyses were carried out for the square encircled selected areas in Figures 2c-2d, and the results are shown as insets. These FFT-SAED patterns display a high degree of crystallinity, especially for region c near the film surface, which shows single-crystal-like sharp diffraction spots (inset of Figure 2c). The measured lattice spacings demonstrate a tetragonal symmetry: the out-of-plane lattice parameters in Figures 2c and 2d are c =4.114 Å and 4.121 Å, respectively, and the corresponding in-plane lattice parameters are a=4.053 Å and 4.048 Å. These values match well with those from the standard PDF card (PDF#70-4060) for a tetragonal MPB PZT (Zr/Ti=52/48) (a=4.055 Å, c=4.11 Å). The film strain εf can be calculated using the equation below: [23]

$$\varepsilon_f = (a - a_0) / a_0 \quad (1)$$

where a represents the lattice parameter of the PZT film, a_0 is the corresponding bulk lattice parameter. Calculations show that from the bottom region d to the surface region c, ε_f in the out-of-plane direction decreases from 0.27% to 0.10%, while the compressive strain in the in-plane direction also decreases from -0.17% to -0.05%. This small negative in-plane strain is consistent with the well-matched CTEs between PZT and the Ti substrate. In addition, the relaxation of the film strain from its bottom to surface is well explained in the literature for a thick film. Such a small in-plane compressive strain in the PZT film lays a crucial foundation for the optimization of its piezoelectric performance [24].

 doi:10.20944/preprints202604.1515.v1

To quantitatively analyze the chemical composition of the PZT film, TEM-EDS point and line scans were performed. Figure 3a displays a representative EDS point-scan spectrum acquired from the middle bulk region of the PZT layer (labeled ① in Figure 2a). Only the elements of O, Ti, Zr, and Pb were detected in Figure 3a (no detectable signals from other elements), verifying the effective role of a diffusion barrier played by the LNO buffer layer. A representative EDS point analysis revealed that the Zr/Ti atomic ratio is approximately 1.084, matching well with the theoretical value of 1.083 at the MPB. Additionally, the Pb/O atomic ratio is approximately 0.35, close to the 1:3 stoichiometric ratio (≈0.33), confirming the formation of a high-quality perovskite phase. The EDS line scan in Figure 3b, acquired along the white arrow in Figure 2a, shows the spatial elemental distribution across the PZT/LNO/Pt/Ti heterostructure. The PZT film occupies the position range from 0 to ~1.27 μm, where Pb, Zr, Ti, and O all show a relatively uniform and stable distribution, confirming its compositional stability. The LNO buffer layer is located in the position range from ~ 1.27 μm to ~1.4 μm, where signals of La and Ni are mainly distributed. The position range between ~1.4 μm and ~1.9 μm corresponds to the Pt bottom electrode layer, where both strong Pt signals and noticeable Ti signals were observed. The latter showed two characteristic distribution zones. The first zone peaked in the middle of the Pt layer (at a position ~ 1.6 μm), decaying on both sides while being accompanied by an oxygen signal with a similar distribution. Such observations indicate diffusions of both elements into the Pt layer and a chemical reaction at where they encountered. The second zone was located near the interface between the Pt layer and the Ti substrate, showing a decaying Ti signal as it penetrated into Pt. This zone corresponds to the transition layer observed in Figure 2a. Correspondingly, the Pt signal showed the opposite trend as that of the diffused-in Ti. It ramped up away from the first zone ("TiO_x" zone), where it showed a minimum. The Pt signal reached a stable high value (as for bulk Pt) at the Pt/LNO interface before taking a nosedive to a noise-level. On the other hand, heading towards the Ti substrate from the "TiO_x" zone, the Pt signal firstly peaked at its bulk value and then slowly decayed down to zero through the Pt/Ti "transition layer" zone. Lastly, in the position range beyond ~1.9 μm, the Ti substrate was reached and displayed a sole signal above the noise level, indicating a successful suppression of oxygen penetration.

 doi:10.20944/preprints202604.1515.v1

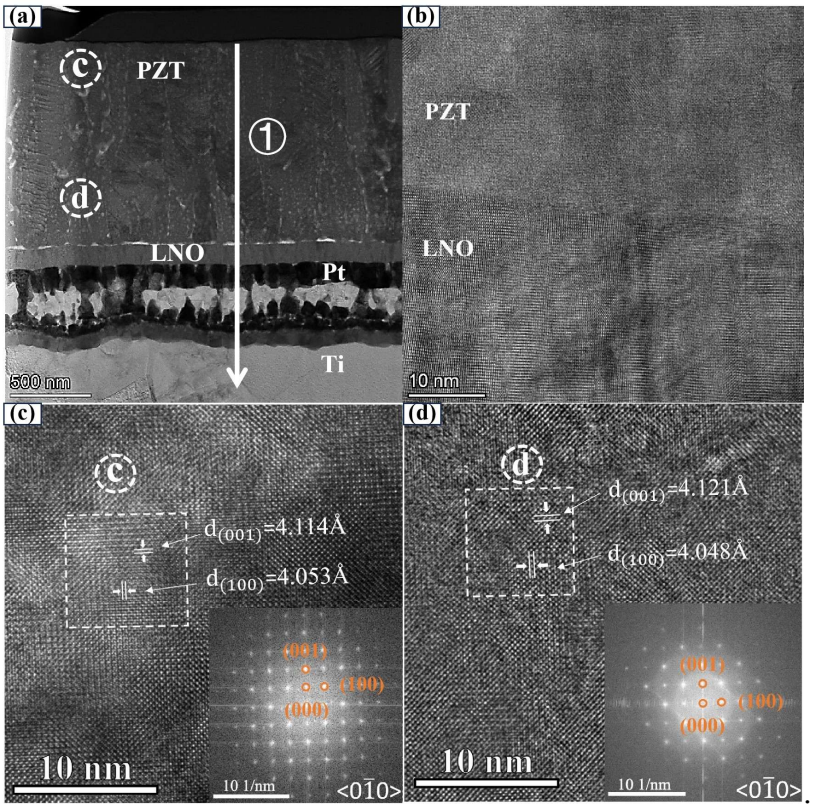

Figure 2. Nanoscale structural analysis (a) cross-sectional bright field TEM image, (b) HRTEM image of the PZT/LNO interface, (c-d) High-magnification lattice images with corresponding Fast Fourier Transformed Selected Area Diffraction Patterns (FFT-SAED, insets).

Moreover, High-Angle Annular Dark-Field (HAADF) imaging was performed on the cross-section of the PZT/LNO/Pt/Ti heterostructure, together with EDS plane-scan of individual elements (Figures 3c-3j). In Figures 3f and 3i, the interdiffusion of Pt and Ti were verified, while in Figure 3j, the oxidation of diffused Ti in the Pt layer was also validated. Meanwhile, the Pt/LNO interface is comparatively sharp and flat, with the LNO layer uniformly covering the Pt grains and serving as a conductive buffer for the PZT layer on top. It is noted that the diffusion of Pt towards the PZT film was effectively blocked by the LNO layer (Figure 3i) [11]. The latter shows chemically abrupt top and bottom boundaries, within which the La and Ni signals (Figures 3g, 3h) are strictly confined, revealing a ~120 nm thickness for this buffer layer. Consequently, a smooth and clean-cut LNO/PZT interface was achieved, consistent with the regular TEM result (Figure 2b). Additionally, the elemental maps for Pb, Zr, and Ti demonstrate a homogeneous distribution throughout the PZT layer without any signs of segregation or composition fluctuation (Figures 3d, 3e, 3f). They also all show a sharp depleted region at where the LNO layer exists, reaffirming the role of a diffusion barrier that LNO played in addition to a crystallographic template. Together with the result shown in Figure 3b and 3i, it is concluded corresponding EDS elemental plane-scan profiles of the PZT/LNO/Pt/Ti heterostructure. that there is no discernible upward Pt migration into the PZT or downward diffusion of the Pb/Zr/Ti atoms. It is noted that, the Zr signal found in the Pt/Ti zone came from the interfering signal of Mα for Pt (~2.048 keV), which significantly overlaps with Lα for Zr (~2.042 keV) [25]. Lastly, using quantitative EDS, the Ti/O atomic ratio in the "TiO_x zone" was estimated to be ~ 1:1.22, endowing a x value of ~1.22 (inset of Figure 3b). This observation indicates that the titanium oxide is sub-stoichiometric and hence conductive. Therefore, in the PZT/LNO/Pt/Ti heterostructure, not only the oxidation of the Ti substrate was suppressed, but the conductive electrode was also preserved

 doi:10.20944/preprints202604.1515.v1

with a pristine Pt/LNO interface (TiO_x was buried inside Pt). This is ideal for promoting an outstanding and robust piezoelectric performance in the (001)-textured PZT film.

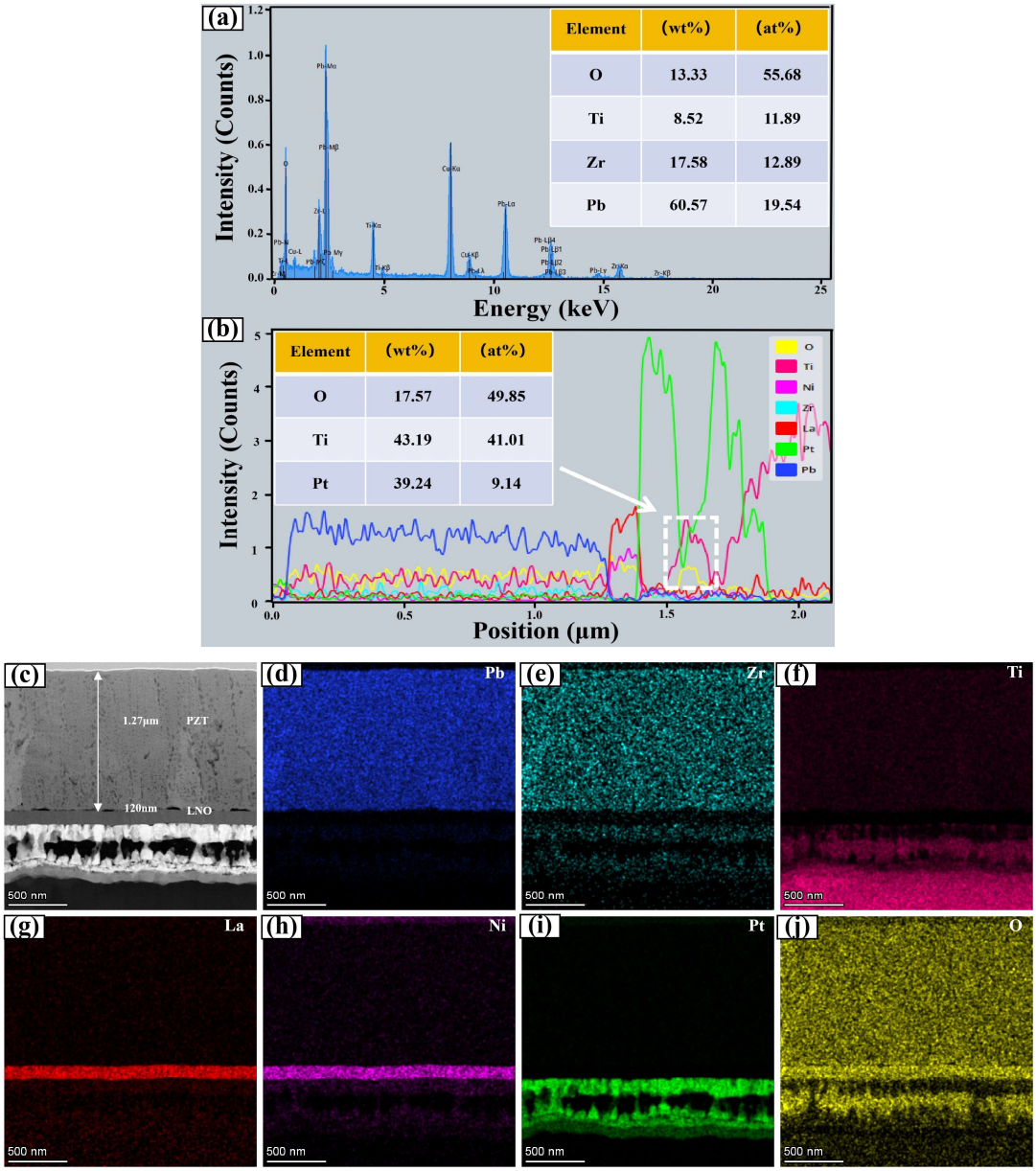

Figure 3. Nanoscale chemical composition analysis (a) TEM EDS spectra with a quantitative analysis (inset), collected from region① of Figure 2a, (b) EDS line-scan spectrum collected along the marked arrow direction in Figure 2 a (inset: quantitative analysis of the Ti-rich region inside the Pt electrode layer), (c) cross-sectional HAADF-STEM image, and (d)-(j).

With these nanoscale EDS results, the beneficial role played by the LaNiO3 layer in stabilizing the PZT/Pt and Pt/Ti interfaces during thermal processing can be interpreted from both thermodynamic and kinetic perspectives. Thermodynamically, because LNO shares the perovskite structure with PZT, the PZT/LNO interface exhibits lower interfacial energy than PZT grown directly on metallic electrodes. This structural compatibility reduces the nucleation barrier for the perovskite phase and promotes the formation of a dense, well-textured film. In addition, the mixed ionic–electronic conductivity of LNO allows partial equilibration of oxygen chemical potential across the interface during thermal processing. Such equilibration reduces the thermodynamic driving force for

 doi:10.20944/preprints202604.1515.v1

oxygen transport toward the titanium substrate, thereby suppressing Ti substrate oxidation and mitigating interfacial reactions (forming sub-stoichiometric, conductive TiO_x, instead of insulating TiO2, inside the Pt electrode layer). These effects collectively contribute to stabilizing the PZT/LNO/Pt/Ti heterostructure during rapid thermal crystallization in a O2 atmosphere. Such a boosted stabilization can also be understood from a kinetic perspective. In polycrystalline thin films, oxygen transport is often dominated by grain-boundary and defect-assisted diffusion pathways. Direct growth of PZT on metallic electrodes like Pt typically produces interfaces with significant structural mismatch, which can introduce interfacial defects that act as fast diffusion channels. The introduction of a perovskite LNO buffer layer improves structural compatibility with PZT and promotes the formation of a dense film with fewer interfacial defects and grain-boundary pathways. Consequently, the effective oxygen diffusion toward the titanium substrate is reduced. This promoted growth of PZT on LNO also enabled a rapid thermal crystallization via RTP, which further curtailed the supply of oxygen toward the Ti substrate. Moreover, due to this LNO-enabled, rapidly ramping and short duration RTP step, the out-diffusion of Ti was greatly mitigated and eventually stopped by the formation of TiO_x inside the Pt electrode layer.

Based on the EDS results and the above analysis, it can be inferred that during RTP in an oxygen atmosphere, Pt grain boundaries were activated at an elevated temperature. This activation enables Ti atoms to diffuse along these intergranular pathways [12,26,27], and react with the diffused-in oxygen. Consequently, sub-stoichiometric titanium oxide (TiO_x) grew in-situ in a semi-continuous fashion (expanding laterally and vertically from the grain boundaries of Pt), until being self-limited due to lack of reactant supply. In the middle of the Pt layer and being a conductor itself [26,28], the resulted TiO_x "band" acted as a sink for O and a diffusion barrier for Ti without ruining the bottom electrode. Not only did it protect the Ti substrate by preventing further penetration of oxygen, but it also kept the metallic Ti within the Pt electrode, hence maintaining the chemical stoichiometry of the MPB PZT film (Zr/Ti=52/48). The activation of the intergranular diffusion of Ti and the subsequent reaction need a high processing temperature, which is supported by our previous work on low-temperature sputter-deposition (@450 °C) of $BiFeO_3$ films onto Ti substrates [14]. In this work, no detectable amount of diffused Ti was revealed in the Pt bottom electrode layer. Therefore, the rapidly ramping, short-duration RTP process, enabled by the introduction of the LNO buffer layer, is not only a crystallization step for PZT with a reduced thermal budget, but also a thermal treatment leading to the formation of a diffusion sink/barrier buried inside the Pt electrode layer. The resulting dual-buffer and dual-barrier configuration—where the LNO layer acts as the orientation-defining template and final diffusion-shield [11], while the Pt layer induces the (100) LNO template growth [29], and a self-limiting oxidative reaction leading to the formation of a diffusion barrier/sink for Ti and O—is the key to preserve the chemical integrity of both PZT and the Ti substrate, while at the same time allow the formation of a desirable crystallographic orientation. Consequently, optimal ferroelectric and piezoelectric properties are expected for the PZT/LNO/Pt/Ti heterostructure.

The high degree of (001)-textured crystallinity revealed in the microstructural analysis translates directly into superior ferroelectric properties. Figure 4a displays the polarization-electric field (*P-E*) hysteresis loop of the PZT film measured at room temperature at a maximum electric field of 461 kV/cm. The film exhibits a well-saturated, square-shaped hyste- resis loop with a large remnant polarization (P_r) of ~ 61 μC/cm² and a saturation polarization (P_s) of ~ 91 μC/cm², as well as a small coercive field (E_c) of ~56 kV/cm. Such a large P_r, one of the highest reported for PZT films integrated on metallic substrates, is a direct manifestation of the highly (001)-oriented crystalline structure, which allows for an efficient collective domain switching under an electric field applied along the film normal. The switching current curve (inset of Figure 4a) shows two sharp, symmetric peaks at the positive and negative coercive fields, confirming that the measured polarizations mostly came from intrinsic ferroelectric polarizations rather than leakage artifacts. To measure the intrinsic ferroelectric polarization of the PZT film, we performed PUND (Positive Up, Negative Down) pulse polarization measurements, which can eliminate the contribution to polarization charges from leakage current and linear dielectric capacitance. The PUND test results, i.e., the measured switchable

 doi:10.20944/preprints202604.1515.v1

polarization ΔP as a function of the applied electric field, are presented in Figure 4b. At the same maximum electric field as that of the *P-E* loop test (~ 461 kV/cm), ΔP is ~ 113 μC/cm², which is nearly twice the remnant polarization Pr (~61 μC/cm²) from the *P-E* loop. This result confirms that the PZT film on Ti possesses an outstanding ferroelectric property. Moreover, Figure 4c presents the frequency-dependent dielectric property [30]. The film demonstrates a high relative dielectric constant (ε_r) of ~1612 at 1 kHz and maintains a low dielectric loss (tanδ) below 0.06 over a broad frequency range of [1 kHz, 1 MHz] [31]. The characteristic "butterfly" shape of the ε_r-*E* curve (inset of Figure 4c) is a hallmark of the film's strong ferroelectric nature. Furthermore, the PZT film's electrical integrity is confirmed by a low leakage current density of 2.1 × 10^{-5} A/cm² at 120 kV/cm (Figure 4d), a result of its dense microstructure and chemical purity.

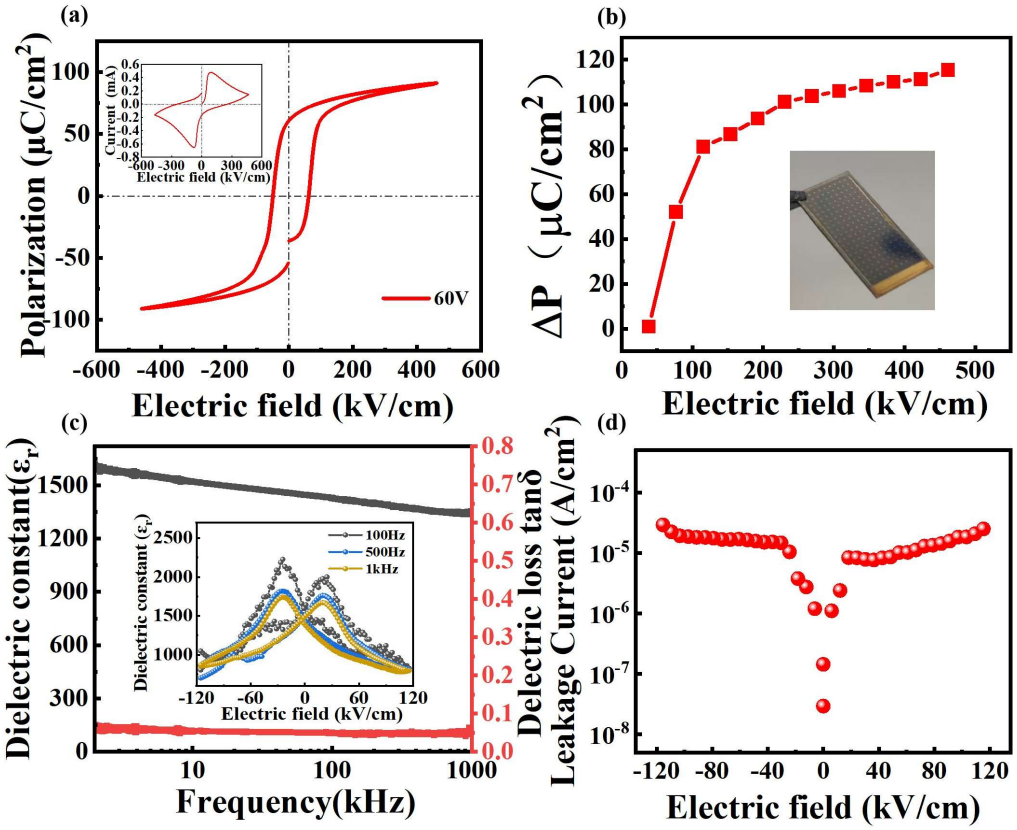

Figure 4. Electrical properties (a) *P-E* hysteresis loop, (b) electric field-dependent pulsed polarization (ΔP) measurement results via PUND (inset is a picture of the sample for electrical characterizations), (c) frequency dependent dielectric constant and loss tangent (tanδ), with inset showing a typical ferroelectric ε_r–*E* loop with a "butterfly" shape, (d) leakage current density (*J*–*E*) curve of the (001)-oriented PZT thick film on Ti.

Lastly, the magnitudes of the transverse piezoelectric coefficients ($|e_{31,f}|$) of the PZT film were measured from the tip displacements of a cantilever beam (Figure 5a) diced from the Pt/PZT/LNO/Pt/Ti heterostructure. As shown in Figure 5b, the tip displacement increases almost linearly with an increasing AC voltage, reaching ~1.36 μm at 16 V. The corresponding $|e_{31,f}|$ maintains at a stable high value, ranging between 6.1 to 6.3 C/m² when ramping up from 0V to 16V. It only increased slightly (from 6.3 to 6.7 C/m²) during ramping down (16V→1V), which can be attributed to a fully poled polarization state [32]. This remarkable pseudo-linearity suggests that the piezoelectric response is dominated by the intrinsic piezoelectric effect, characteristic of a highly (001)-oriented PZT film [32–34]. Furthermore, δ and $|e_{31,f}|$ as functions of the piezoelectric actuation cycles were displayed in Figure 5c. After 1.2 × 10^6 actuation cycles under an applied AC voltage of 6 V, reductions in δ and $|e_{31,f}|$ were very small (~4%), indicating an excellent fatigue resistance. The ac voltage used

 doi:10.20944/preprints202604.1515.v1

for measurements presented in Figures 5b and 5c was at 100 Hz, far away from the resonance frequency of the cantilever beam. The latter was determined by a frequency sweep (Figure 5d) to be ~ 860 Hz. This is to ensure quasi-static conditions for the measurement of $e_{31,f}$.

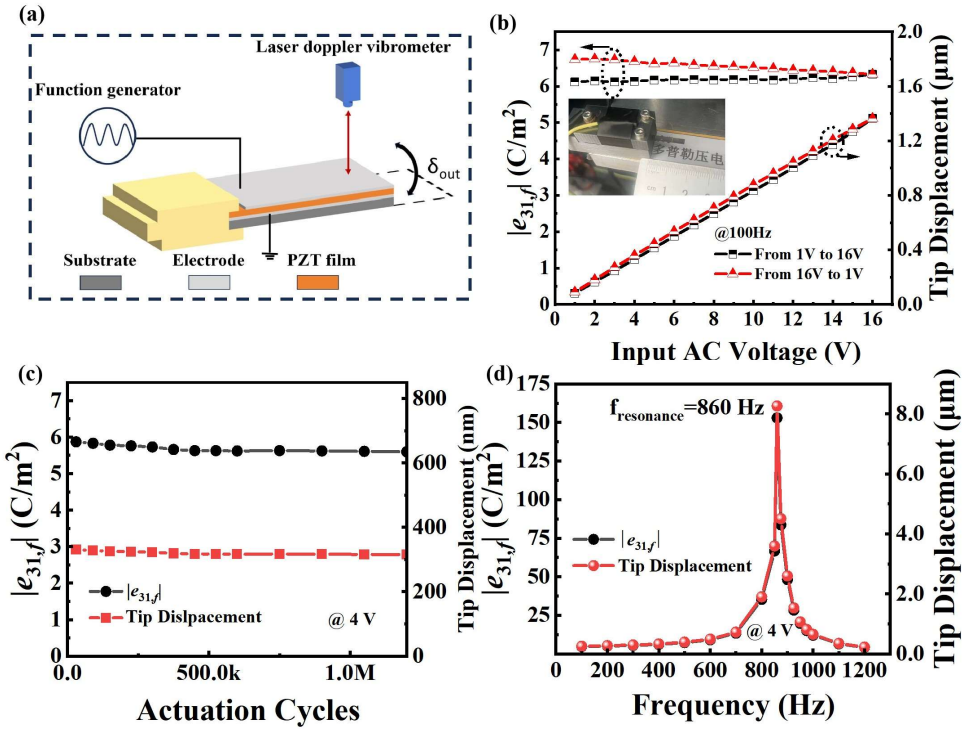

Figure 5. Transverse piezoelectric properties of the (001)-oriented PZT thick film on Ti. (a) Schematic of the piezoelectric measurement setup, (b)-(d) tip displacement and corresponding transverse piezoelectric coefficient ($|e_{31,f}|$) as functions of (b) amplitude of an input AC voltage (inset is a picture of the cantilever beam sample in the fixture for piezoelectric characterization), (c) the number of piezoelectric actuation cycles, (d) the exciting frequency of the input ac voltage (@ a fixed AC voltage of 4V).

Table 2 compares the key performance metrics of our PZT film against other commonly used ferroelectric films [6,10,14,35], i.e., PZT and $BiFeO_3$ (BFO), on Ti substrates (there is no reported data for the integration of (K,Na)NbO_3 films on Ti). Most notably, our PZT film achieved much higher polarization values (P_r~61 μC/cm²) than its PZT peers, together with a much larger dielectric constant (ε_r~1612). Based on the positive correlations between these two parameters and the transverse piezoelectric coefficient $e_{31,f}$ [32,36], a superior $e_{31,f}$ coefficient was expected and that's what was revealed experimentally. $|e_{31,f}|$ is ~6.7 C/m² in a fully poled state, and ~ 6.1 C/m² for the unpoled state. This transverse piezoelectric property significantly outperforms its PZT peers and lead-free counterpart of $BiFeO_3$. This performance boost can be attributed to a synergistic effect from the three factors below:

Table 2. This is a table. Tables should be placed in the main text near to the first time they are cited.

Source	This work	[6]	[10]	[35]	[14](BFO)
$E_c\ (kV/cm)$	56	70	45	—	145
$E_b\ (kV/cm)$	850	—	—	—	—
$P_s\ (\mu C/cm^2)$	91	35	—	27	84
$P_r\ (\mu C/cm^2)$	61	20	0.5	—	72
ε_r	1612	506	120	534	273
Converse $e_{31,f}$ (C/m^2)	6.1-6.7	3.6-4.3	—	—	2.2

 doi:10.20944/preprints202604.1515.v1

1. The LNO buffer layer, which ensures a high (001) orientation with an optimal polar axis alignment, and at the same time acts as a diffusion barrier for PZT and Pt electrode.
2. The "rapidly ramping, short duration" RTP process, which yields a dense, highly crystalline microstructure essential for the electrical and piezoelectric performances, while at the same time limits the inter-layer diffusion and ensures the chemical integrity of the PZT film, as well as the highly reactive Ti substrate.
3. Matching CTEs between the Ti substrate and PZT film, helps to minimize the film's residual stress. A slightly compressive residual stress is beneficial to maintain a high electric polarization, a crucial foundation for the electrical and piezoelectric performances of a ferroelectric film.

4. Conclusions

In summary, high-quality, (001)-oriented PZT thick films (~1.27 μm) were successfully integrated onto Ti substrates, via a two-step process combining a low-temperature RF sputter-deposition (@400 °C) with a RTP. The introduction of a conductive LNO growth template proved critical in lowering the nucleation energy barrier for the (001) perovskite PZT. Moreover, the LNO layer acted synergistically with the RTP to suppress substrate oxidation and mitigate interfacial diffusions and chemical reaction. Consequently, the resulting (001)-textured PZT film exhibits a dense columnar grain microstructure, and delivers outstanding electrical and piezoelectric performances. A large remnant polarization of ~ 61 μC/cm^2, a low leakage current (J≈2.1×10^{-5} A/cm^2 @ 120 kV/cm), and a high dielectric constant (ε_r ~ 1612 @ 1 kHz) were demonstrated by the PZT film. Most notably, a large transverse piezoelectric coefficient $e_{31,f}$ of ~ -6.7 C/m^2 was achieved, significantly outperforming the reported piezoelectric films grown on Ti. This work effectively resolves the thermal budget conflict, lying between achieving a high degree of crystallinity in the PZT film and avoiding deterioration of devices on reactive metal substrates, thereby establishing a scalable and cost-effective pathway for flexible piezo-MEMS devices.

Author Contributions: Conceptualization, J.O., H.C. and Z.G.; formal analysis, Z.G.; Investigation, Z.G. and S.C.; writing—original draft preparation, Z.G.; writing—review and editing, J.O., H.C. and Z.L.; supervision, J.O. and H.C.; Funding acquisition, H.C.; All authors have read and agreed to the published version of the manuscript.

Funding: Funding: This work was supported by the National Natural Science Foundation of China (NSFC, Grant Nos. 92463306), the Natural Science Foundation of Shandong Province (Grant Nos. ZR2022ZD39, ZR2022ME031, ZR2023QB119), the Education Department of Hunan Province/Xiangtan University (Grant No. KZ0807969), and the Pilot Project to Integrate Science, Education and Industry of Qilu University of Technology (Grant No. 2024RCKY030).

Data Availability Statement: The article includes all data.

Acknowledgments: J. Ouyang is grateful for research support from Seton Hall University.

Conflicts of Interest: The authors declare no conflict of interest.

References

1. Y. Yue, F. Qu, Q. Zheng, Z. Hu, I. Abrahams, H. Yan, G. Viola, B. Han, M. Krynski, T. Honda, Structural Origin of Morphotropic Phase Boundary in Advanced Perovskite Ferroelectric Oxides, J. Am. Chem. Soc. 148 (2026) 7827–7836.
2. M.-F. Tsai, J. Jiang, P.-W. Shao, Y.-H. Lai, J.-W. Chen, S.-Z. Ho, Y.-C. Chen, D. P. Tsai, Y.-H. Chu, Oxide Heteroepitaxy Based Flexible Ferroelectric Transistor, ACS Appl. Mater. Interfaces 11 (2019) 26642–26651.
3. T. Sheng, Q. He, Z. Xu, C. Wei, Z. Yu, B. Li, T. Xu, Heterogeneous Integration of PZT Thin Films on Flexible Polyimide Substrates via a ZnO Release Process for Energy Harvesting, ACS Appl. Electron. Mater. 8 (2026) 1360–1366.
4. X. Lu, Y. Wu, J. Chen, Y. Chen, C. Yin, X. Wu, D. Xiao, A high liftoff speed insect-scale aerial robot direct-driven with piezoelectric bimorph PZT actuator, Chin. J. Aeronaut. 38 (2025) 103494.

 doi:10.20944/preprints202604.1515.v1

5. C. Li, H. Yu, T. Shu, Y. Zhang, C. Wen, H. Cao, J. Xie, H. Li, Z. Xu, G. Zhang, Z. Yu, H. Li, L. Liu, Y. Shi, F. Qiu, D. Dai, PZT optical memristors, Nat. Commun. 16 (2025) 6340.
6. K. Kanda, I. Kanno, H. Kotera, K. Wasa, Simple Fabrication of Metal-Based Piezoelectric MEMS by Direct Deposition of Pb(Zr, Ti)O_3 Thin Films on Titanium Substrates, J. Microelectromech. Syst. 18 (2009) 610–615.
7. S. H. Kweon, E.-J. Kim, G. Tan, I. Kanno, Compositional Modification of Epitaxial Pb(Zr,Ti)O_3 Thin Films for High-Performance Piezoelectric Energy Harvesters, Adv. Mater. Interfaces 11 (2024) 2300634.
8. X. Wang, Y.-C. Wang, B. Peng, J. Deng, Y. Yang, W. Sun, Z. Wang, Thickness dependence of $PbZr_{0.52}Ti_{0.48}O_3$ thin film ferroelectric parameters, Nano Energy 107 (2023) 108161.
9. G. Yi, Z. Wu, M. Sayer, Preparation of Pb(Zr,Ti)O_3 thin films by sol gel processing: Electrical, optical, and electrooptic properties, J. Appl. Phys. 64 (1988) 2717–2724.
10. A. Bose, M. Sreemany, Influence of processing conditions on the structure, composition and ferroelectric properties of sputtered PZT thin films on Ti-substrates, Appl. Surf. Sci. 289 (2014) 551–559.
11. Q. Zou, H. E. Ruda, B. G. Yacobi, Improved dielectric properties of lead zirconate titanate thin films deposited on metal foils with $LaNiO_3$ buffer layers, Appl. Phys. Lett. 78 (2001) 1282–1284.
12. K. Sreenivas, I. Reaney, T. Maeder, N. Setter, C. Jagadish, R. G. Elliman, Investigation of Pt/Ti bilayer metallization on silicon for ferroelectric thin film integration, J. Appl. Phys. 75 (1994) 232–239.
13. B. Lin, Q. Wei, H. Hua, D. Qi, H. Zhang, S. Wang, Y. Li, High-performance PZT piezoelectric films on glass with $LaNiO_3$ buffer layer, Ceram. Int. 51 (2025) 18567–18574.
14. J. Yan, J. Ouyang, H. Cheng, P. Yan, Low temperature deposition of $BiFeO_3$ films on Ti foils for piezoelectric applications, Scr. Mater. 204 (2021) 114152.
15. X. Hao, J. Zhai, X. Yao, Improved dielectric properties of (110)-preferred (Pb, La)(Zr, Sn, Ti)O_3 antiferroelectric thin films on metalorganic decomposition-derived $LaNiO_3$ buffer layer, J. Crystal Growth 311 (2008) 90–94.
16. J. F. Shackelford, W. Alexander, CRC Materials Science and Engineering Handbook, 3rd ed., CRC Press, Boca Raton (2001).
17. Y. Wang, H. Cheng, J. Yan, N. Chen, P. Yan, F. Yang, J. Ouyang, Large piezoelectricity on Si from highly (001)-oriented PZT thick films via a CMOS-compatible sputtering/RTP process, Materialia 000 (2019) 100228.
18. N. Wakiya, T. Azuma, K. Shinozaki, N. Mizutani, Low-temperature epitaxial growth of conductive $LaNiO_3$ thin films by RF magnetron sputtering, Thin Solid Films 410 (2002) 114–120.
19. Y. Wang, J. Ouyang, H. Cheng, Y. Shi, T. Nishikado, I. Kanno, High performance $LaNiO_3$-buffered, (001)-oriented PZT piezoelectric films integrated on (111) Si, Appl. Phys. Lett. 121 (2022) 182902.
20. D. Das, L. Sanchez, J. Martin, B. Power, S. Isaacson, R. G. Polcawich, I. Chasiotis, Control of Ferroelectric and Linear Piezoelectric Response of PZT Films through Texture, J. Am. Ceram. Soc. 101 (2018) 2023–2032.
21. Z. Duan, X. Shi, Y. Cui, Y. Wan, Z. Lu, G. Zhao, Ferromagnetic, ferroelectric and magnetoelectric properties of (001)-oriented $Pb(Zr_{0.52}Ti_{0.48})O_3/La_{0.67}Sr_{0.33}MnO_3$ composite films deposited on Si substrates using chemical solution deposition, J. Alloys Compd. 698 (2017) 276–283.
22. Wang Y, Zhu H, Xue Y, Yan P, Ouyang J, Microstructure evolution with rapid thermal annealing time in (001)-oriented piezoelectric PZT films integrated on (111) Si, Materials, 16 (2023) 2068.
23. A. L. Roytburd, J. Ouyang, A. Artemev, Polydomain structures in ferroelectric and ferroelastic epitaxial films, J. Phys.: Condens. Matter 29 (2017) 163001.
24. T. A. Patel, K. Co, R. J. Hebert, S. P. Alpay, Ferroelectric films on metal substrates: The role of thermal expansion mismatch on dielectric, piezoelectric, and pyroelectric properties, J. Appl. Phys. 126 (2019) 134103.
25. A. Bose, T. Maity, S. Bysakh, A. Seal, S. Sen, Influence of plasma pressure on the growth characteristics and ferroelectric properties of sputter-deposited PZT thin films, Appl. Surf. Sci. 256 (2010) 6205–6212.
26. C. Millon, C. Malhaire, C. Dubois, D. Barbier, Control of the Ti diffusion in Pt/Ti bottom electrodes for the fabrication of PZT thin film transducers, Mater. Sci. Semicond. Process. 5 (2003) 243–247.
27. G. Velu, D. Rémiens, Electrical Properties of Sputtered PZT Films on Stabilized Platinum Electrode, J. Eur. Ceram. Soc. 19 (1999) 2005–2013.

 doi:10.20944/preprints202604.1515.v1

28. T. Leichtweiss, R. A. Henning, J. Koettgen, R. M. Schmidt, B. Holländer, M. Martin, M. Wuttig, J. Janek, Amorphous and highly nonstoichiometric titania (TiOx) thin films close to metal-like conductivity, J. Mater. Chem. A 2 (2014) 5692–5701.
29. Yang C C, Chen M S, Hong T J, Wu C M, Wu J M, Wu T B, Preparation of (100)-oriented metallic LaNiO3 thin films on Si substrates by radio frequency magnetron sputtering for the growth of textured Pb(Zr0.53Ti0.47)O3, Appl. Phys. Lett. 66(1995) 2643.
30. S.-T. Mo, K.-M. Feng, J.-L. Pang, K. Ouyang, L.-M. Jiang, Q. Yang, B. Zhang, J. Jiang, All-inorganic transparent $Hf_{0.85}Ce_{0.15}O_2$ ferroelectric thin films with high flexibility and stability, Nano Res. 16 (2023) 5065–5072.
31. K. I. Hnatiuk, Y. F. Zabashta, M. M. Lazarenko, S. A. Alekseev, K. S. Yablochkova, M. V. Ushcats, R. V. Dinzhos, L. Y. Vergun, D. A. Andrusenko, A. N. Alekseev, L. A. Bulavin, Dielectric Relaxation in Nanocrystals: A Scale Effect, J. Phys. Chem. C 127 (2023) 12107–12117.
32. Y. Wang, H. Cheng, J. Yan, N. Chen, P. Yan, J. Ouyang, Nonlinear electric field dependence of the transverse piezoelectric response in a (001) ferroelectric film, Scripta Mater. 189 (2020) 84–88.
33. C. Zhao, X. Jiang, C. Chen, Y. Chen, L. Wang, L. Sun, R. Zeng, N. Tu, X. Huang, X. Nie, Major contributor to high-performance in $Na_{0.5}Bi_{2.5}Nb_2O_9$-based piezoelectrics: Domain wall motion, Ceram. Int. 51 (2025) 41672–41679.
34. G. Hennessey, T. Peters, P. Tipsawat, M. Checa, L. Collins, S. Trolier-McKinstry, Domain wall motion across microstructural features in polycrystalline ferroelectric films, Acta Mater. 250 (2023) 118871.
35. H. Dong, M. Chen, H. Zhu, Y. Huang, Q. Ding, J. Feng, Effects of thermal strain on electric properties of lead zirconate titanate thin films upon $LaNiO_3$ coated base metal plates, Ceram. Int. 46 (2020) 1867–1873.
36. H. Luo, M. Niu, H. Zhu, L. Li, H. Cheng, C. Liu, J. Li, Y. Zhao, C. Zhang, X. Cao, I. Kanno, Q. Chi, J. Ouyang, Temperature-modulated crystallographic orientation and electrical properties of $BiFeO_3$ thick films sputtered on $LaNiO_3$/Pt/Ti/SiO_2/Si for piezo-MEMS applications, J. Adv. Ceram. 13 (2024) 1943–1954.